FINITE ELEMENT ANALYSIS OF THE FORCES DEVELOPED ON LINEAR INDUCTION MOTORS

Roberto A. H. de Oliveira[1], Dietmar Berger [2], Ludwig Schultz[2,3], Richard M. Stephan[1] and Antônio C. Ferreira[1]
[1]Electrical Engineering Department, Federal University of Rio de Janeiro, Rio de Janeiro - Brazil
[2]Institute for Metallic Materials, Leibniz Institute for Solid State and Materials Research Dresden, Dresden - Germany
[3]Faculty of Mechanical Science and Engineering, Technical University of Dresden, Dresden - Germany
email: raholiveira@ufrj.br, d.berger@ifw-dresden.de, l.schultz@ifw-dresden.de, richard@dee.ufrj.br and ferreira@coep.ufrj.br

***Abstract* - Superconducting magnetic levitation (SML) vehicles use a levitation technology based on the diamagnetic property of Y-Ba-Cu-O blocks and the magnetic field of Nd-Fe-B magnets. Brazilian SML project, MagLev-Cobra uses for the propulsion a short primary linear induction motor (LIM) with a squirrel cage secondary type. SupraTrans 2, the Germany MagLev vehicle, uses a short primary motor with secondary with copper plate and back-iron. Both motors assembly contribute to increase the levitation force. Brazilian tests with one levitating module on a 12 m track have shown a variation of the levitation height with the motor loading. In this paper, 2D - 3D finite element analysis will be used to study lateral, levitation and traction forces. Simulation and experimental results will be compared.**

***Keywords* – Finite Element Analysis, Linear Induction Motor, Superconducting Magnetic Levitation.**

NOMENCLATURE

A_{cs}	active surface of the primary core
A_c	conductor cross-section
$\hat{B}_g$	magnetic flux density in the airgap
B_{my}	peak value of the normal component of magnetic flux density in the airgap
B_{mx}	peak value of the tangential component of magnetic flux density in the airgap
E_1	voltage induced
τ	pole pitch
g	airgap
L_i	effective width of the primary core
α_i	ratio average-to-peak of the B_{my}
k_{w1}	primary winding factor for the fundamental harmonic
σ_f	form factor of the primary electromotive force
Γ	utilization factor $\frac{k_w}{\sqrt{2}} A_c \hat{B}_g$

I. INTRODUCTION TO SML VEHICLES

Efforts on research and development of the Brazilian superconducting magnetic levitation project, MagLev-Cobra, started in 2000. Figure 1 shows the vehicle, developed by COPPE / UFRJ, using the levitation technology based on the interaction of high temperature superconductors YBCO and the magnetic field produced by Nd-Fe-B magnets [1]. The levitation force due to the superconductors, as used in this project, has been studied for several years by the authors [2]. The cryostat used in the vehicle supports forces of up to 2250N [3] and each module uses 6 cryostats, with a total carrying capacity of up to 1350 kg per module. The vehicle will be able to carry 30 passengers and will be composed of 4 levitating modules, each one 1.5 meter long. Currently, a full scale prototype, composed of one module and running on a 12 meter track, is being used to identify technical characteristics of the system as well as to allow the design of several auxiliary systems. The vehicle uses a linear induction motor topology called "Double-C" or "C-shape". Both primary and secondary use ferromagnetic core and are arranged so that the normal attractive force contributes to the vehicle levitation.

Fig. 1. : MagLev-Cobra vehicle developed by COPPE/UFRJ.

Figure 2 shows the SupraTrans 2, another vehicle based on the same levitation technology (SML) described above. There is a repulsion force between the primary and secondary harnessed to increase the levitation force on the vehicle. The first generation of SupraTrans (ST), SML vehicle developed in Germany by the Leibniz Institute for Solid State and Materials Research Dresden (IFW-Dresden), used linear doubly-fed motor and the primary fed by a supercapacitor's bank inside the vehicle. The secondary of the ST was fed by a source power with different frequency of the primary. The second generation of the ST, the SupraTrans 2 (ST2), uses a LIM with secondary back-iron and fed by wireless power transfer. One point of interest is the interaction between the traction and the levitating system.

This paper presents measurements of the levitation height variation with the motor loading and will compare the results with 2D and 3D finite element simulation. Finally, it intends to validate the methodology of linear induction motors analysis by Finite Element Method (FEM). After its validation,

Fig. 2. : SupraTrans 2 vehicle developed by IFW-Dresden.

the FEM will be used to help traction motor design in future projects.

II. FINITE ELEMENT METHOD

A model was developed in two (2D) and three (3D) dimensions of the linear induction motors and is presented in sections III.A and III.B, respectively. The calculations were performed for the condition of locked primary, which is the simplest condition, in both LIM topologies. The linear motor windings are connected in star (Y). The electromagnetic force in the longitudinal direction was called traction force (F_x). The normal force (F_y) acts on the Y-axis direction and the lateral force (F_z) acts on the Z axis. The F_z occurs when there is an asymmetric position between primary and secondary and due to the uneven distribution of induced currents in the secondary.

III. LINEAR INDUCTION MOTORS

The mechanical power of the LIM is composed of two parts F_c and F_e [4]. Generally, the force on the LIM is given by (1), where F_c is the force per pole on the central part and F_e, the force per pole on the end part. There are two poles in the end regions (1). F_e and F_c are given by (2) and (3), respectively. The number of poles in the central region is defined by $p_c = 2p_p - 2$, where p_p is the number of pole-pairs. The force with ideal length and width ($l_{1i} = \alpha 2p_p\tau$) and ($b_{1i} = b_1 + 0.7g$), respectively, will be given by (4).

$$F = \sum_{p_c} F_c + \sum_{2} F_e = \sum_{p_c} F_c + 2F_e \quad (1)$$

$$F_e = F_c \frac{w_e^2}{w_c^2} = \frac{1}{4} F_c \quad (2)$$

$$F_c = \tau b_{1i} \Gamma \quad (3)$$

$$F = l_{1i} b_{1i} \Gamma = \alpha 2p_p \tau b_{1i} \Gamma \quad (4)$$

Figure 4 shows the relationship α, according to (5), between length of the primary and number of pole-pairs. Linear motors with few numbers of poles, for instance $p < 8$, presents low performance. The relationship between width and the length winding of the primary ($\lambda = b_1/\tau$) can be used to increase the performance of the LIM. The better geometric relationship is given by expression $b_1 > \tau$ [4], [5]. The effective surface area of the laminated primary is given by (6). The total length is formed by $2p_p\tau + b_{te}$, where b_{te} is not necessarily equal b_t, illustrated on Figure 3. The ideal length of the primary follows the presented relationship (7).

$$\alpha = \frac{2p_p - 1.5}{2p_p} \quad (5)$$

$$A^x = b_{1i} l_{1i} \quad (6)$$

$$l_{1i} = 2p_p\tau \quad (7)$$

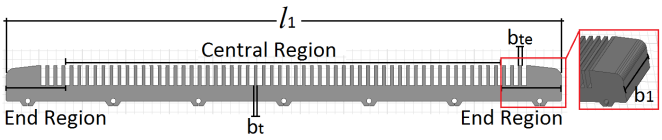

Fig. 3. : Illustration of the primary LIM "Double-C".

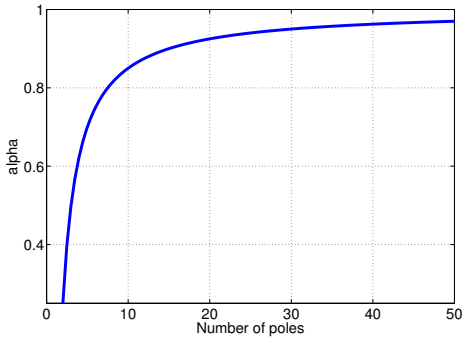

Fig. 4. : α-factor.

A. LIM "Double-C" - MagLev-Cobra

For the propulsion of the vehicle, a linear induction motor (LIM) with a short primary and long secondary squirrel cage is used. The part containing the excitation winding is called Primary, and the part containing the squirrel cage is called Secondary. The primary and secondary of the MagLev-Cobra motor are presented in Figure 5 and 6, respectively. The primary has 3 phases and 6 poles and the secondary, of a squirrel cage type, is composed of several modules 1.51m long each. It is necessary to electrically connect the cage along the trajectory.

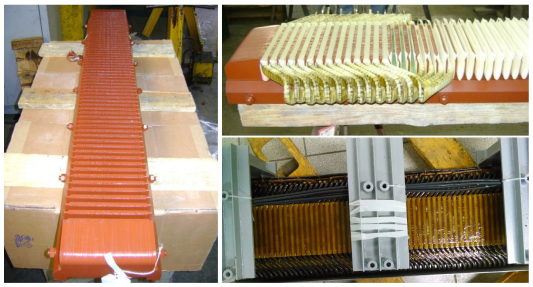

Fig. 5. : Primary of the LIM "Double-C".

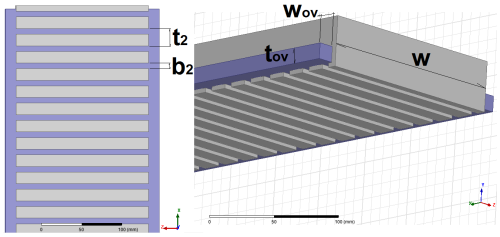

Fig. 6. : Secondary of the LIM "Double-C" design.

Force Result by FEM in the LIM "Double-C"

Figures 7 - 8 show the 2D and 3D models of LIM "Double-C", respectively, presented in section III.A, developed on Maxwell Software. The primary winding is connected in Y and is excited with a three-phase voltage with amplitude of 420V@25Hz. Traction and attraction forces in 2D model were calculated for different air gaps, as g=8mm; 12mm; 16mm and 20mm. The 3D model uses g=8mm to calculate traction, attraction and lateral forces.

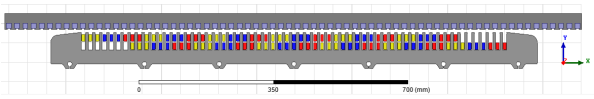

Fig. 7. : FEM 2D-Model of the MagLev-Cobra LIM.

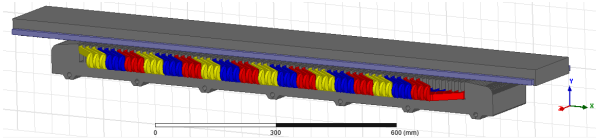

Fig. 8. : FEM 3D-Model of the MagLev-Cobra LIM.

Figures 9 and 10 show the traction and attraction force developed by LIM "Double-C" with continuous secondary section. The results show the natural decrease of the motor efficiency with increasing air gap. Figure 11 shows the forces developed by 3D model LIM "Double-C". Figure 12 show the airgap magnetic flux density (B) in LIM "Double-C" operating with 420V@25Hz and differents air gaps. The traction force experimental tests were performed with the locked primary for different air gaps and ratio V/f constant. The results for airgaps between 8mm and 24mm are presented in Figure 13.

The results for the attractive force obtained with static test is shown in Figure 14. The static experimental attraction force is measured with a load cell installed between the floor and the primary of the LIM. Airgap of 8mm has been chosen and the frequency varied between 1Hz to 6Hz.

Figure 15 show the contribution of the attraction force to the levitation during a dynamic test. The test was performed by measuring of the vehicle height with static levitation. The ultrasonic sensor (*BUS M18K0-XAER-040-S92K*), used to measure the gap, was positioned at ≈12mm on the ground. An acceleration ramp was imposed and the speed vehicle reached 0.9m/s and traveled a distance of 4.5m, during experimental attraction dynamic tests. The voltage applied was 50V@3Hz and average increase of ≈4mm was measured, i.e., the dynamic

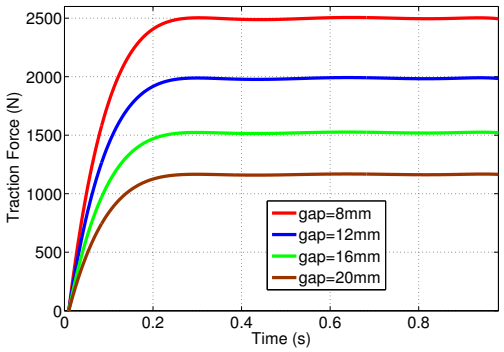

Fig. 9. : Traction Force (F_x) LIM "Double-C" - 2D model.

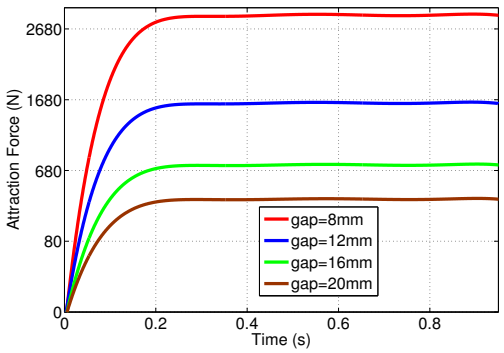

Fig. 10. : Attraction Force (F_{ya}) LIM "Double-C" - 2D model.

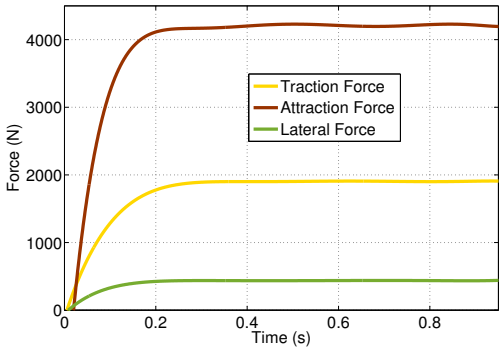

Fig. 11. : F_x, F_{ya} and F_z developed with g=8mm - 3D model.

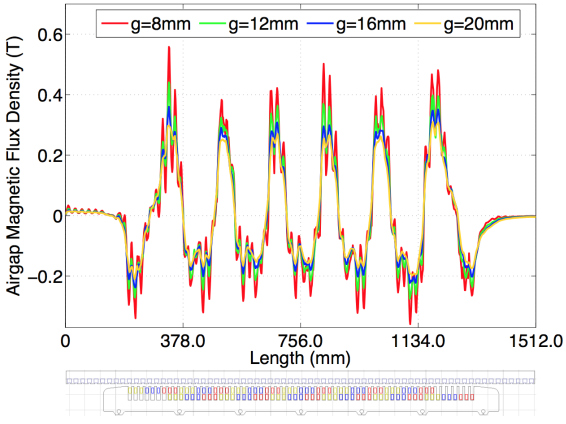

Fig. 12. : Airgap Magnetic Flux Density (T) - 2D model.

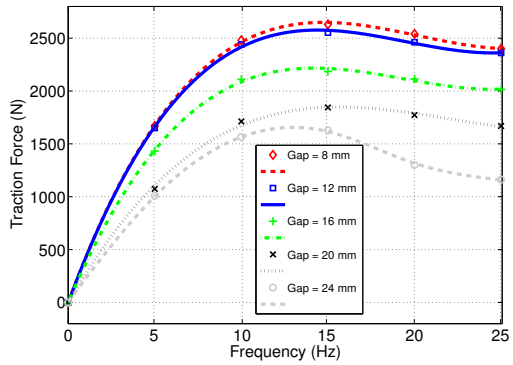

Fig. 13. : Traction Force Experimental Results.

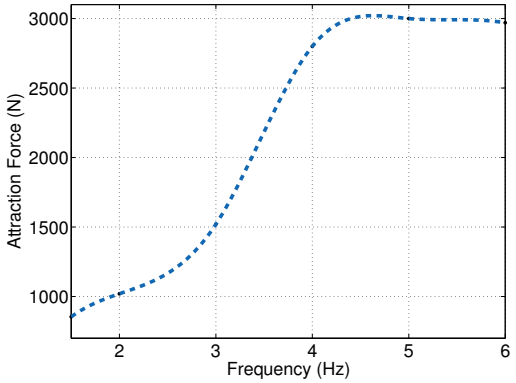

Fig. 14. : Attraction Force in Static Test with gap=8mm.

levitation was 33.3% higher than the static levitation.

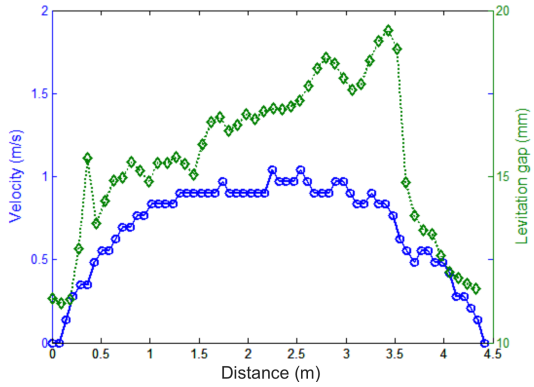

Fig. 15. : Experimental Results in Dynamic Test.

A comparison between 2D, 3D and experimental results are compiled in Table I. The 2D simulation shows a reasonable accuracy and experimental result of traction force is 3.6% lower than the simulated result. Attraction experimental force was 0.36% higher than the 2D simulated results. The 3D model simulation results showed discrepancy. The traction force was 20.5% lower than the experimental results and the attraction force was 39.9% higher than the experimental results. This difference can be attributed partially to the developed model, mesh and/or numerical problems. The 3D model numerical calculation is slower than 2D model. It is evidence the effectiveness and speed of 2D simulations by ANSYS Maxwell to linear systems electromagnetic model. A depuration in the 3D model is important, however the slowness convergence of the results will not be improved.

TABLE I: Results Compiled - LIM "Double-C" Topology

Forces[1]	**2D**	**3D**	**Experimental**
Traction (N)	2489.70	1908.00	2403.00
Attraction (N)	2987.00	4197.00	2998.00
Lateral (N)	-	436.00	-

[1] $airgap = 8mm$

B. LIM "Back-Iron" - SupraTrans 2

The SupraTrans 2 uses a short primary linear induction motor (LIM) with a copper-plate back-iron secondary. It's a three phase machine with 57 coils forming 20 poles. The Primary of the LIM of the SupraTrans 2 is presented in Figure 16 which also shows complete model of the LIM.

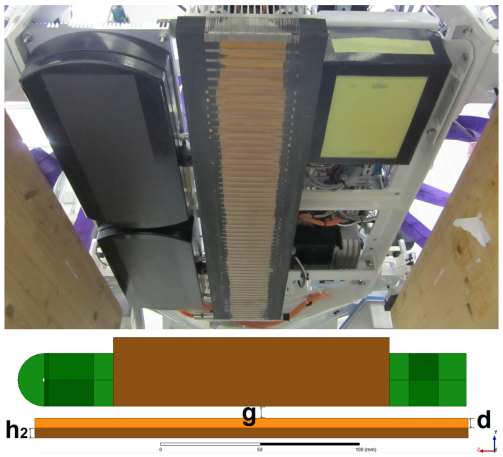

Fig. 16. : LIM "Back-Iron".

Force Results by FEM in the LIM "Back-Iron"

Figures 17 - 18 show the 2D and 3D models of LIM "Back-Iron", respectively. Initially the calculations were performed for the condition of locked primary. The LIM "Back-Iron" primary winding is excited with a three-phase voltage with amplitude of 380V@50Hz. The LIM windings are connected in star (Y).

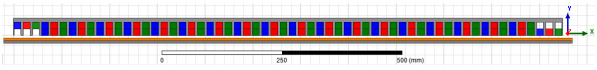

Fig. 17. : FEM 2D-Model of the SupraTrans2 LIM.

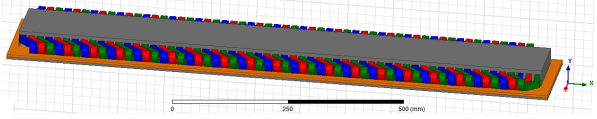

Fig. 18. : FEM 3D-Model of the SupraTrans2 LIM.

The traction and repulsion forces in 2D model were calculated with g=6mm, but different secondary type: Cu=5mm, Cu=10mm, Al=5mm and Al=10mm. Figures 19 - 20 show the traction and repulsion forces developed by 2D model of the LIM "Back-Iron" with continuous secondary section. In 3D model, the voltage applied was 380V@50Hz and figure 21 shows the traction, repulsion and lateral forces.

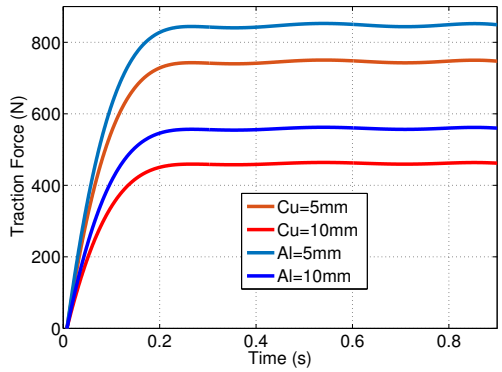

Fig. 19. : Traction Force (F_x) LIM "Back-Iron" - 2D model.

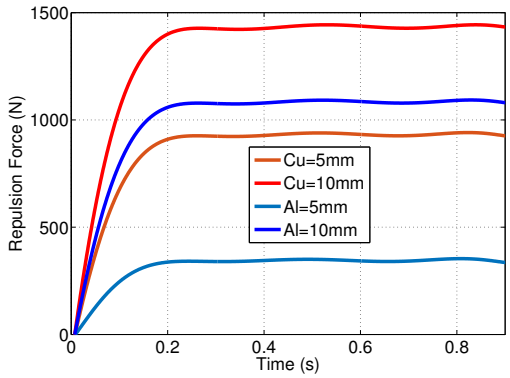

Fig. 20. : Repulsion Force (F_{yr}) LIM "Back-Iron" - 2D model.

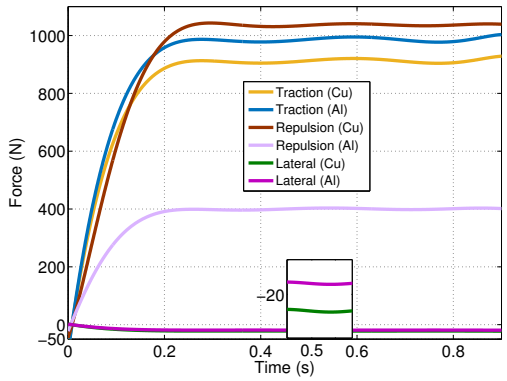

Fig. 21. : F_x, F_{ya} and F_z with Cu and Al=5mm - 3D model.

Figure 22 shows airgap magnetic flux density on the secondary with copper and aluminum. Secondary with copper presents B bigger than aluminum secondary. The traction force tests were performed with the locked primary for different air gaps and ratio V/f constant. Figures 23 and 24 show experiental traction forces and simulated repulsion force, with coppe-plate back-iron, respectively.

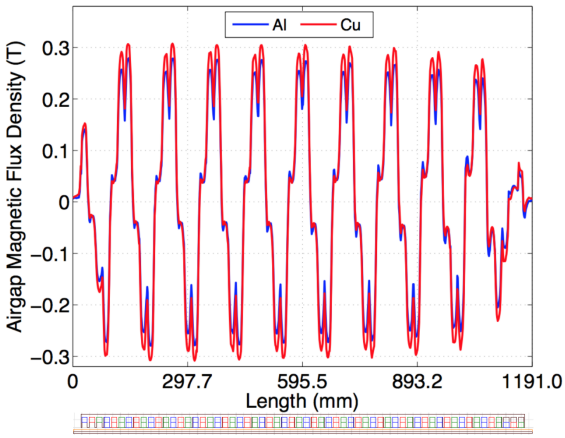

Fig. 22. : Airgap Magnetic Flux Density (T) - 2D model.

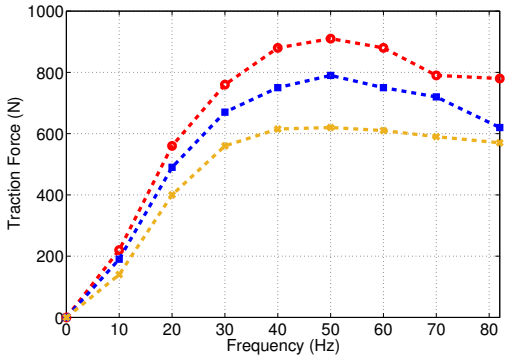

Fig. 23. : Experimental Result of the Traction Force (F_x) with differents airgaps (copper plate = 5mm).

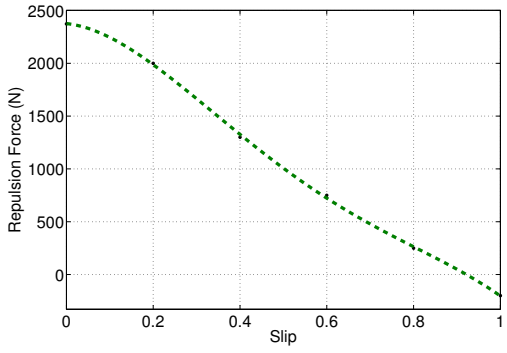

Fig. 24. : Simulated Result of the Repulsion Force (F_z) with g=8mm (copper plate = 5mm).

Table II presents the compiled force results. The experimental results of traction force and repulsion force with copper cage was 5.9% and 15.7% higher than 2D simulated results,

respectively. Traction force obtained with 3D simulation was 14.5% higher than the experimental results and the simulation repulsion force was 6.2% lower.

TABLE II: Results Compiled - LIM "Back-Iron" Topology

	F_x (N)	F_{yr} (N)	F_z (N)
2D[1]			
$Cu = 5mm$	742.90	926.70	-
$Cu = 10mm$	459.40	1428.00	-
$Al = 5mm$	844.10	341.40	-
$Al = 10mm$	556.80	1079.00	-
3D[1]			
$Cu = 5mm$	904.60	1032.00	-22.04
$Al = 5mm$	977.70	397.10	-18.79
Experimental[1]			
$Cu = 5mm$	790.00	1100.00	-

[1] $airgap = 6mm$

IV. CONCLUSIONS

The analysis of the linear induction motor using the finite element method presented important 2D results that can be compared with reasonable accuracy to the experimental results. Table III shows the complete results for each motor and conditions. The reliable models allow analysis by finite elements methods to unwanted effects, eddy currents, and can help minimize the end effects for high-speed operations. Dynamic analysis of the motor should be performed to better understand the particular effects of linear motors. The analysis contribute to future projects of special machines with necessary preliminary data of magnetic flux density, force and airgap for efficient operation.

The short analysis presented in section III shows the relationship between the number of poles, geometry and efficiency of the LIM. Variation of winding type, polar pitch, squirrel cage material, the primary current frequency, among other aspects may help to design more efficient machines adapted to the desired operation. Due to geometry of the primary used in MagLev-Cobra, noted a large region of null air gap magnetic flux. This characteristic impoverishes the weight and force relationship.

The distributed winding (LIM "Double-C") produces a sinusoidal magnetic flux when compared with the motor with concentrated winding (LIM "Back-Iron"), to according Figures 12 and 22, reducing MMF harmonics. The contribution of the attraction force, known from experimental results for low speed, was presented. Finally the lateral force does not affect significantly "Double-C" or "Back-Iron" performance. Due to geometric asymmetry not considered on models, the lateral force must be greater and bench tests need to be done.

Future work plan to evaluate the fluid air flow and increase the thermal efficiency of the motor. The 3D models need improvement, due to results questionable when compared with measurements. Reduced losses by Joule effect and possible improvements in the geometry and motor characteristics can be implemented from these results. Increase of the normal and tangential magnetic flux density is necessary.

TABLE III: Comparison - LIM's

Parameters	**MagLev-Cobra**	**SupraTrans 2**
Voltage	$420V - (Y)$	$380V - (Y)$
Current	$53A$	$45A$
Frequency	$25Hz$	$50Hz$
Power	$10HP$	$7.2HP$
Number of the Poles	6	20
Pole Pitch, τ	$156.0mm$	$57.5mm$
Air Gap	$8mm$	$6mm$
Factor λ	1.06	2.43
$\alpha-$Factor	0.75	0.92
Traction Force	$2403N$[1]	$910N$[1]
Repulsion Force	–	$1100N$[2]
Attraction Force	$2998N$[1]	–
Lateral Force	$436N$[2]	$-22.04N$[2]
Density[3] F_x	$52.5 \times 10^3 N/m^3$	$102.7 \times 10^3 N/m^3$
Primary	**MagLev-Cobra**	**SupraTrans 2**
Length	$1270mm$	$1150mm$
Height	$106mm$	$35mm$
Yoke Width	$166mm$	$140mm$
Winding Width	$340mm$	$220mm$
Index of Protection	$IP - 23$	$IP - 54$
Weight	$132kg$	$46kg$
Secondary	**MagLev-Cobra**	**SupraTrans 2**
Length	$1510mm$	$1190mm$
Height	$53mm$	$10mm$
Width	$231mm$	$250mm$
Weight	$53.98kg/m$	$11.26kg/m$

[1] Experimental Results [2] Simulation Result

[3] Force Density (primary volume: $l \times w \times h$ - core and winding.)

ACKNOWLEDGEMENT

This work was suppoorted in part by CAPES, BNDES, CNPq and FAPERJ.

REFERENCES

[1] R. M. Stephan et al. Maglev-cobra: An urban transportation solution using hts-superconductors and permanent magnets. *Proc. of MAGLEV 2008*, pages 1–4, 2008.

[2] R. De Andrade et al. Performance of nd-fe-b and ferrite magnets in superconducting linear bearings with bulk ybco. *Applied Superconductivity, IEEE Transactions on*, 13(2):2271–2274, 2003.

[3] G.G. Sotelo et al. Tests with one module of the brazilian maglev-cobra vehicle. *Applied Superconductivity, IEEE Transactions on*, 23(3):3601204–3601204, 2013.

[4] Peter-Klaus Budig and Germar Müller. *Drehstromlinearmotoren*. Verlag Technik, 1978.

[5] Jacek F Gieras. *Linear Induction Drives*. Number 30. Oxford University Press, 1994.